

VISIBLE-LIGHT-INDUCED Fe-DOPED ZnO MAGNETIC PHOTOCATALYST NANOPARTICLES FOR DEGRADATION OF METHYLENE BLUE

M. YOUSAF^a, H. M. RAFIQUE^a, M. AMIN^a, S. M. RAMAY^b, S. ATIQ^{c*},
N. S. ALZAYED^b, S. A. SIDDIQI^d

^aDepartment of Physics, University of the Punjab, Lahore-54590, Pakistan

^bDepartment of Physics and Astronomy, College of Science, King Saud University,
P. O. Box 2455, Riyadh 11421, Saudi Arabia

^cCentre of Excellence in Solid State Physics, University of the Punjab,
Lahore-54590, Pakistan

^dInterdisciplinary Research Centre in Biomedical Materials, COMSATS Institute
of Information Technology, Off Raiwind Road, Lahore-54600, Pakistan

Visible-light-induced Fe-doped zinc oxide photocatalysts with nominal compositions $Zn_{1-x}Fe_xO$ ($x=0.0, 0.05$) via sol-gel combustion method have been investigated. The structural, thermal, morphological, elemental, magnetic and optical properties have been investigated systematically using X-ray diffractometer, thermogravimetric analysis, field emission scanning electron microscope equipped with energy dispersive X-ray spectroscopy, physical properties measurement system and UV/vis-spectrophotometer, respectively. Wurtzite-type hexagonal crystal structure was evident from the diffraction analysis. The doping of Fe^{3+} at Zn-site in ZnO helped to reduce its bandgap energy, attributed to the creation of an extra level near band edges. The synthesized materials exhibited an enhanced photocatalytic activity visualized using degradation of methylene blue under the irradiation of visible-light. Pseudo-first-order rate law was also applied to study the reaction kinetics of methylene blue catalyzed by visible-light irradiation.

(Received November 4, 2016; Accepted January 27, 2017)

Keywords: Magnetic photocatalysts; Fe-doped ZnO; Sol-gel preparation;
RT ferromagnetism

1. Introduction

In the last decade, ZnO and TiO₂ based semiconductors have shown significant magnetic characteristics at room temperature (RT) or at low temperatures when some transition-metal cations such as Fe, Ni, Co or Mn are doped in them [1]. Although these materials have attained considerable attention due to their vast applications in spintronics [2-4] yet they have also played a key role to get rid of organic pollutants via photodegradation, becoming promising materials in the field of photocatalysis [5].

For an efficient semiconductor photocatalyst, the valence and conduction bands of the catalysts play an important role. To get maximum efficiency, these bands need to be adjusted such that the oxidation potential of the hydroxyl radical [$E(H_2O/OH) = 2.8$ V vs normal hydrogen electrode (NHE)] and the reduction potential of superoxide radical [$E(O_2/O_2^-) = 0.28$ V vs NHE] should lie within the band gaps of the catalysts. Since, the band gaps of ZnO and TiO₂ are closer to the hydroxyl oxidation potential; therefore, these materials are considered more efficient photocatalysts [6]. Band gap of ZnO is 3.2 eV, which is analogous to TiO₂ and considered an alternative catalyst for degradation of organic pollutants. Moreover, ZnO absorbs larger portion of the UV light of the solar spectrum as compared to TiO₂ making it a more suitable material for

*Corresponding author: satiq.cssp@pu.edu.pk

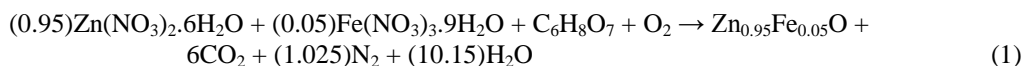
photocatalytic applications [7]. Solar energy spectrum accounts 46% for visible and 6% for UV-light of the total energy reaching earth from the sun. Rest of the spectrum is covered by infrared region [8-9]. Therefore, ZnO photocatalysts in pure form can only utilize a very small portion of sunlight. Many thanks to a large amount of solar energy from visible portion that reaches the earth's surface annually, it is necessary to synthesize such type of photocatalysts having maximum bandgap of 3.1 eV [10].

Although, low cost and complete mineralization of ZnO and TiO₂ adds to their characteristic benefits, these materials are immensely discharged in water. Their recovery is not easy and hence poses much loss of the materials [11]. A large number of solid-liquid separation techniques exist that can be used to separate photocatalysts but an additional cost is required for this step. Therefore, magnetic photocatalysts have advantages over photocatalysts because their recovery is possible by magnetic force [10]. Many attempts have been reported to convert UV sensitive materials to visible-light absorbents. A more common approach is to incorporate elements like nitrogen, carbon, sulfur, cobalt, silver, gold, platinum and ruthenium into the UV-active photocatalyst [12]. Alternatively, one can contemplate the development of materials with narrow band gaps [13-15]. Recently, some researchers have doped transition metals, for example Co²⁺, Ni²⁺ and Fe³⁺ in ZnO to enhance the optical characteristics [16-19]. Different concentrations of Fe³⁺ ions in ZnO have separated the electron-hole pair by decreasing the bandgap, which shift the absorption spectrum from UV to visible region [20]. Sol-gel technique offers numerous advantages over other methods. For instance, simplicity of processing, single-phase formation and the enhanced homogeneity of the prepared samples [21].

In this present work, we have synthesized pure and Fe-doped ZnO with the nominal composition Zn_{0.95}Fe_{0.05}O by sol-gel combustion technique. The method has been adopted acknowledging its effectiveness to prepare low cost and phase pure oxide materials in a quick time. The effect of Fe³⁺ contents in ZnO under the irradiation of visible-light has been discussed in order to use this composition as a potential photocatalytic material.

2. Materials and methods

Fe-doped ZnO nanocrystallites of the form Zn_{0.95-x}Fe_xO (x = 0.00, 0.05) were prepared using sol-gel auto-combustion route. Analytical grade reagents such as zinc nitrate [Zn(NO₃)₂·6H₂O, 10196-18-6] and iron nitrate [Fe(NO₃)₃·9H₂O, 7782-61-8] were used as starting materials after weighing in proper stoichiometric molar ratios [22]. Citric acid [C₆H₈O₇, 77-92-9] was used as a fuel agent keeping metal nitrates to citric acid ratio of 1 : 2. All the reagents were first separately dissolved in de-ionized water and then mixed together to make a total volume of 50 mL. The solution was placed on a hot plate at 95 °C for about 2 h and stirred magnetically. This led to a brownish xerogel. At the instance, the stirring was stopped and temperature of the hot plate was raised to 300 °C. After a while, the gel was burnt as a result of self-ignited combustion process. As a result, the gel was finally converted to a fine and fluffy powder after an exothermic reaction. The powder samples were calcined at 700 °C to establish the desired crystalline phases. The balanced equation of the reaction can be written as;



Crystal structure and crystallite size of both the samples were determined using a Rigaku Ultima IV X-ray diffractometer utilizing CuK_α line having wavelength 1.5406 Å, in a 2θ range of 20 – 80°. A 300 S II, EXSTAR thermogravimetric analyzer (TGA) was used to check the thermal stability of the samples in the range of 35 to 800 °C, with heating rate of 9 °C per min in air. Fourier transform infrared (FTIR) spectroscopic analysis was carried out using a Bruker Vertex 70 spectrometer with KBr as a reference material. Magnetic parameters were discussed using magnetic hysteresis (M-H) loops obtained at 300 K, using a Quantum Design physical properties measurement system (PPMS) with an applied field of ±10 kOe. The morphological and elemental analyses were carried out using a JSM-6610 field emission scanning electron microscope

(FESEM) equipped with an Oxford Instrument energy dispersive X-ray (EDX) system. A Shimadzu (ISR-2600) UV-spectrometer) equipped with an accessory of diffuse reflection has been employed to record the UV-Vis absorption spectra. Barium sulfate salt was used as a standard to calibrate the system for baseline correction. The absorption spectra were obtained in wavelength range of 200 to 800 nm.

Methylene blue (MB) has been used as a model dye to check its degradation with the as-synthesized visible-light driven photocatalysts. The degradation with as-synthesized catalysts was performed in a glass tube in which 0.25 g of $Zn_{0.95}Fe_{0.05}O$ powder was suspended in 250 ml of MB solution (10mg/l). A 200 W high pressure sodium lamp (Osoram) having output of 400-550 nm wavelengths with 2200 lumen (20 cm away from the photoreactor) was used as a light source. Before irradiation, the suspended solution was sonicated to disperse the catalyst in dye solution. While conducting experiments, the solution was continuously stirred. After irradiating the sample at a given reaction time, the catalyst was filtered from dye solution. Absorbance rate of the dye solution was determined using a UV-vis spectrophotometer and the degradation rate was evaluated by well-known degradation rate equation:

$$\text{Degradation rate (\%)} = (A_0 - A) / A_0 \quad (2)$$

where A_0 is the initial absorbance and A represents the variable absorbance.

3. Results and discussion

Crystal structure of un-doped and Fe^{3+} -doped ZnO at RT, has been analyzed using XRD and the diffraction patterns are shown in the Fig. 1. Intensity peaks were identified at 2θ values of 32.09° , 34.75° , 36.58° , 47.86° , 56.90° , 63.16° , 66.68° , 68.24° and 69.38° which were indexed corresponding to the (100), (002), (101), (102), (110), (103), (200), (112) and (201) planes, respectively. Indexing was performed by employing the procedure as described by Cullity. This confirmed the hexagonal wurtzite-type crystal structure of both the samples, as they were well matched with JCPDS card no. 75-1526, a characteristic crystal structure of ZnO. No extra peak related to any impurity was witnessed. A slight perturbation in the peak position was observed in the magnified diffraction patterns as shown in Fig. 2. This perturbation mainly was caused by the presence of an ion with smaller radii [Fe^{3+} (0.49 Å)] substituted with the ion with relatively greater radii [Zn^{2+} (0.60 Å)], as already been reported [22, 23].

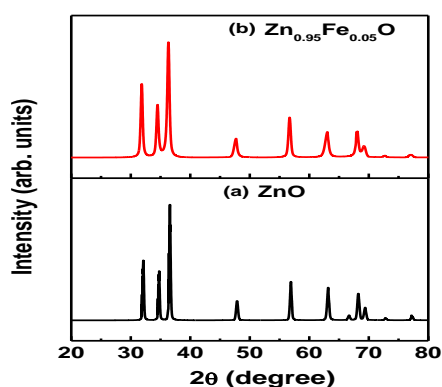


Fig. 1 XRD patterns of (a) ZnO, (b) $Zn_{0.95}Fe_{0.05}O$

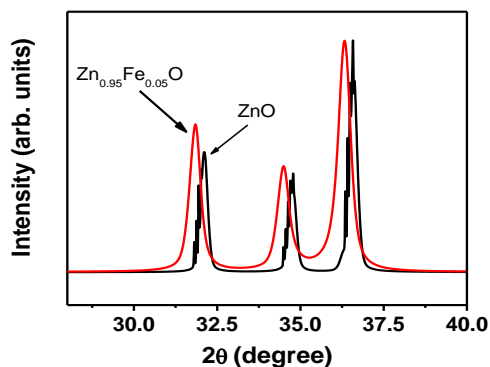


Fig. 2 Magnified XRD patterns of ZnO and $Zn_{0.95}Fe_{0.05}O$

Fig. 3 shows the TGA spectra, recorded to estimate the thermal stability of the synthesized catalysts. The plots reveal a rapid initial weight loss which is attributed to the desorption or drying of water. In the temperature range of 35 – 800 °C, the maximum weight was nearly 1%. This minute loss in weight could be associated with the evaporation of residual water present in the powder samples. Weight loss in case of Fe-doped sample is higher which can be attributed to the presence of additional nitrates in this particular sample [22, 24]. Overall, both the spectra reveal the thermal stability of the samples in a wide temperature range.

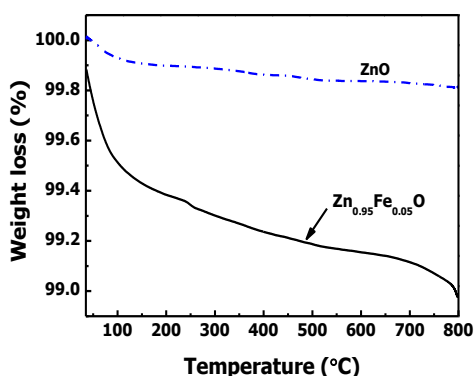


Fig. 3 TGA spectra of pure ZnO and Fe^{3+} doped ZnO

FTIR spectra of ZnO and Fe-doped ZnO is presented in Fig. 4. The results show that there are broad peaks at 3460 cm^{-1} and 1645.2 cm^{-1} . These broad peaks are conventional which are arising due to surface adsorbed water and hydroxyl group, respectively [22, 25]. The most intense peak present at 500 cm^{-1} is a characteristic ZnO peak [26]. The value of absorption band is shifted to 428 cm^{-1} in case of Fe-doped ZnO. This change in peak position is an evident of perturbation in Zn-O-Zn network due to 5% Fe incorporation [24], well in accordance with the diffraction data as revealed by the magnified patterns shown in Fig. 2.

Fig. 5 shows the surface morphology revealed by the FESEM images and the related EDX spectra of both the samples, performed to estimate the elemental composition in the prepared samples. Well-shaped grains with sharply edged grain boundaries were evident in pure ZnO sample as can be seen in Fig. 5(a). The grain sizes were mainly in the range of 80 – 120 nm. Largely, the grains were well embedded into each other. When 5% Fe was doped in ZnO, the grains were mainly spherical in shape, which were well separated from each other. The homogeneously shaped grains were observed to possess sizes in the range of 80 – 100 nm. After incorporating Fe in the ZnO host matrix, apparently the surface became more porous which might enhance the photocatalytic activity. The elemental analysis on the other hand, confirmed the stoichiometric at% and wt% of all the elements present in the samples.

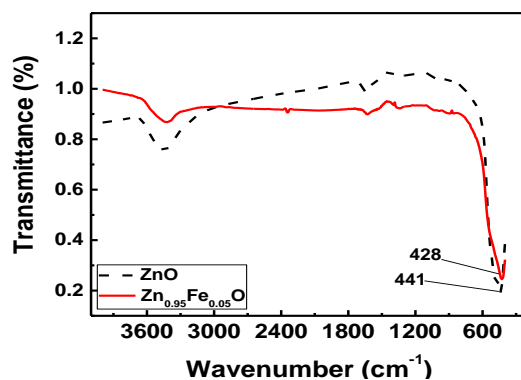


Fig. 4 FTIR spectra of (a) ZnO, (b) $Zn_{0.95}Fe_{0.05}O$

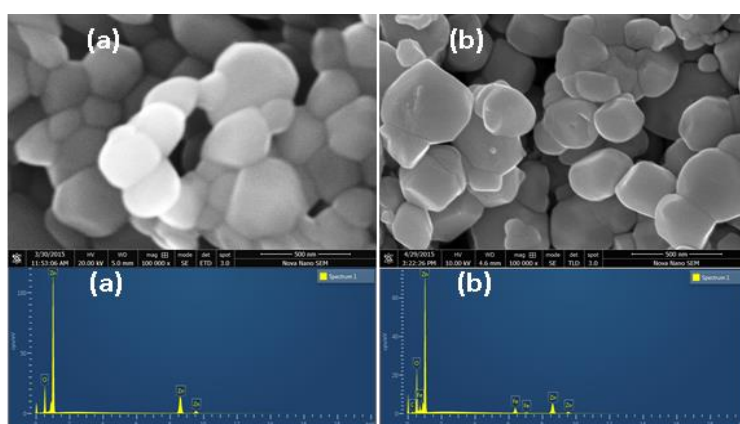


Fig. 5 SEM images and the relevant EDX spectra of (a) ZnO, and (b) $Zn_{0.95}Fe_{0.05}O$

The field dependent magnetic hysteresis loop of Fe-doped ZnO sample obtained at RT by applying a magnetic field of 10 kOe is shown in Fig. 6. Although the sample is not fully saturated at this field yet the hysteresis present in the loop reveal the ferromagnetic nature of the sample. Ferromagnetism in dilute magnetic oxides can be explained using Ruderman-Kittel-Kasuya-Yosida (RKKY) theory [27-29]. According to this theory, ferromagnetic interactions in dilute magnetic semiconductors arise due to exchange interactions between conductive electrons and local spin polarized electrons. Therefore, it is inferred that the doping of Fe^{3+} enhances the free carriers [30] and is mainly responsible for ferromagnetic behavior in Fe-doped ZnO.

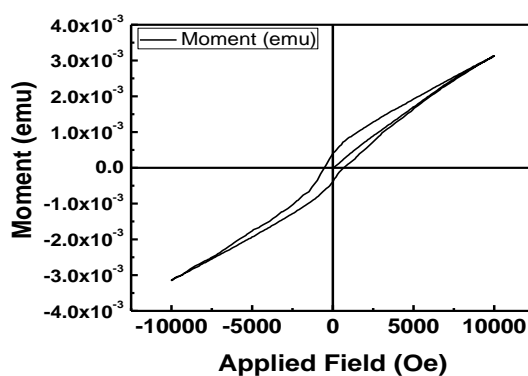


Fig. 6 Field-dependent M-H loop of Fe^{3+} doped ZnO at 300 K

The diffuse reflection spectra of ZnO and Zn_{0.95}Fe_{0.05}O samples were recorded at RT by applying Kubelka-Munk (K-M) theory [24] for bandgap energy (E_g) determination. The K-M technique is based on the relation as given in Eq. 3.

$$F(R) = (1 - R)^2 / 2R = (\alpha h\nu)^n \quad (3)$$

where R is the reflectance and $F(R)$ is proportional to absorption co-efficient ' α '. The value of $n = 1/2$ was used for direct allowed transition. An absorption peak at about 385 nm is obvious in ZnO spectrum which is well in agreement with the intrinsic bandgap energy (3.22 eV) of ZnO. On the other hand, a shift towards visible region (red shift) is observed in the absorption spectra of Fe³⁺-doped ZnO, which in turn, changes the color of catalyst from white to reddish yellow. This red shift is caused by the sp-d exchange interaction between the localized d-electrons of the dopant and the band electrons of ZnO [31-32]. Shifting of bandgap from UV to visible region can also be explained using a well-known effect, termed as Burstein–Mosson effect. In phenomena, Fermi energy level combines with conduction band as a result of increase in carrier concentration, as reported by Nair *et al.* [33]. Fig. 7 shows a plot between $(\alpha h\nu)^{1/2}$ and $h\nu$, exhibiting a bandgap value of 3.1 eV for the Fe-doped ZnO sample [22].

Photo-absorption spectra of the samples is shown in Fig. 8 which reveals the degradation rate of dye solutions with the synthesized catalysts over wavelength range from 400 – 700 nm under different irradiation time (0 – 4 h). The absorption of MB is clearly seen to decrease gradually with increasing irradiation time. However, the extent of this decrease is variable for various catalysts. In case of ZnO, only 28% degradation is witnessed, when the solution is illuminated for 4 h using visible light. In case of Fe-doped sample, it is increased by 59%, as evident in Fig. 8 (b). This means that Fe-doped ZnO catalyst has showed enhanced visible light photocatalytic activity [5, 22], primarily, because of increased separation efficiency of electron-hole pairs. This shows that Zn_{0.95}Fe_{0.05}O is more efficient photocatalyst as compared to ZnO. The trend is in agreement with the corresponding bandgaps of the sample. A decrease in bandgap with Fe³⁺ incorporation in ZnO resulted in more efficient photocatalyst.

Hence, it is inferred from these experimental observations that MB is degraded by increasing irradiation time in the presence of photocatalysts under visible light is caused by an increase life time of excited carriers. This in turn, increases the photocatalytic activity [34].

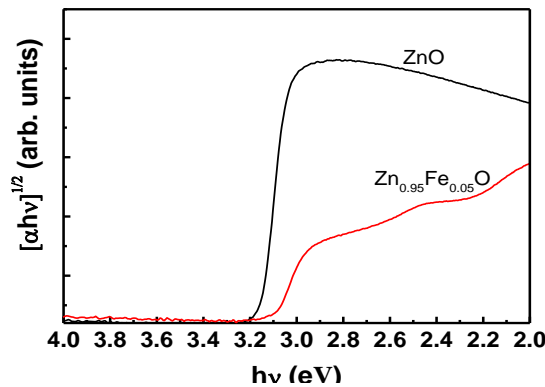


Fig. 7 $(\alpha h\nu)^{1/2}$ vs photon energy ($h\nu$) for ZnO and Zn_{0.95}Fe_{0.05}O

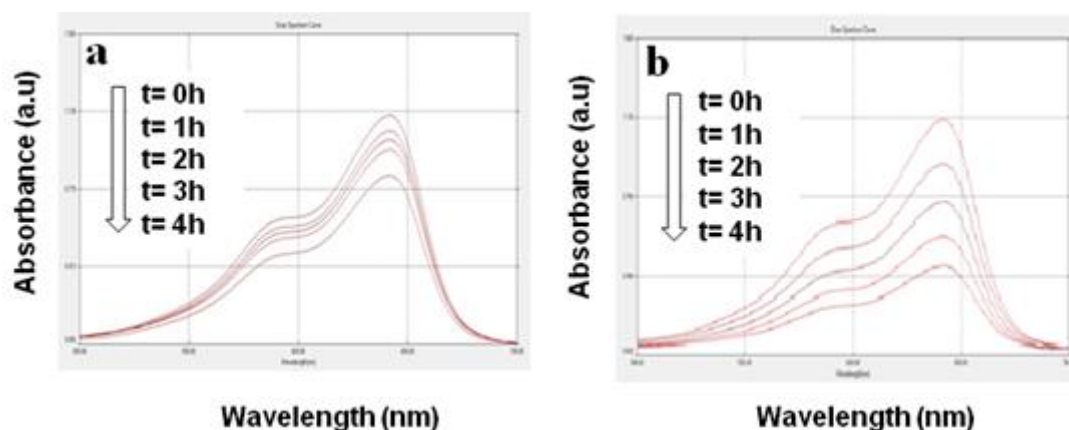


Fig. 8 Time-dependent UV-Vis absorption spectra of (a) ZnO, (b) $Zn_{0.95}Fe_{0.05}O$

4. Conclusions

In this work, we present the synthesis of pure and 5% Fe-doped ZnO using a novel sol-gel auto-ignition route in order to investigate the photocatalytic activity. The data obtained from diffraction revealed a successful incorporation of Fe^{3+} in ZnO as it did not distort the wurtzite-type hexagonal structure.

The VSM analysis confirmed the magnetic nature of the synthesized photocatalysts. A decrease in band is displayed by UV-Vis diffuse reflectance spectrometry in the doped sample. The degradation of MB, an organic dye, was increased when Fe-doped ZnO was used as a photocatalyst. The trend could be attributed to the increased lifetime of excited carriers in consequence of reduced bandgap by Fe incorporation.

It is thus strongly anticipated that the synthesized dilute magnetic oxides would present a promising approach for organic dyes degradation under visible-light solar spectrum.

Acknowledgement

The authors would like to extend their sincere appreciation to the Deanship of Scientific Research at King Saud University for funding this research group no. RG1435-004.

References

- [1] S. Sain, J. Bhattacharjee, M. Mukherjee, D. Das, S. K. Pradhan, *J. Alloy Compd.* **519**, 112 (2012).
- [2] S. W. Jung, S. J. An, G. C. Yi, G. U. Jung, I. S. Lee, S. Cho, *Appl. Phys. Lett.* **80**, 4561 (2002).
- [3] H. Ohno, *Science* **281**, 951 (1998).
- [4] A. F. Abdulrahman, S. M. Ahmed, N. M. Ahmed, M. A. Almessiere, *Dig. J. Nanomater. Bios.* **11**, 663 (2016).
- [5] S. Dong, K. Xu, J. Liu, H. Cui, *Physica B* **406**, 3609 (2011).
- [6] S. Rehman, R. Ullah, A. M. Butt, N. D. Gohar, *J. Hazard. Mater.* **170**, 560 (2009).
- [7] S. Sakthivel, B. Neppolian, M. V. Shankar, B. Arabindoo, M. Palanichamy, V. Murugesan, *Sol. Energ. Mat. Sol. C* **77**, 65 (2003).
- [8] S. Q. Liu, *Environ. Chem. Lett.* **10**, 209 (2012).
- [9] S. Kim, K. Shunsuke, S. Porponth, K. Taizo, N. Tokoi, K. Makoto, *Sol. Energ. Mat. Sol. C* **119**, 214 (2013).
- [10] J. Herrmann, J. Disdier, P. Pichat, S. Malato, J. Blanco, *Appl. Catal. B-Environ.*

- 17**, 15 (1998).
- [11] R. Wang, D. Xu, J. B. Liu, K. W. Li, H. Wang, *Chem. Eng. J.* **168**, 455 (2011).
- [12] E. Casber, V. K. Sharma, X. Z. Li, *Sep. Purif. Technol.* **87**, 1 (2012).
- [13] S. Boumaza, A. Boudjemaa, A. Bouguelia, R. Bouarab, M. Trari, *Appl. Energ.* **87**, 2230 (2010).
- [14] S. Ida, K. Yamada, T. Matsunaga, H. Hagiwara, Y. Matsumoto, T. Ishihara, *J. Am. Chem. Soc.* **132**, 17343 (2010).
- [15] A. Rezaee, H. Masoumbeigi, R. D. C. Soltani, A. R. Khataee, S. J. Hashemiyani, *Desalin. Water Treat.* **44**, 174 (2012).
- [16] H. Chen, J. Ding, F. Shi, Y. Li, W. Guo, *J. Alloy Compd.* **534**, 59 (2012).
- [17] E. Liu, P. Xiao, J.S. Chen, B.C. Lim, L. Li, *Curr. Appl. Phys.* **8**, 408 (2008).
- [18] C. Xia, F. Wang, C. Hu, *J. Alloy Compd.* **589**, 604 (2014).
- [19] D. Fang, K. Lin, T. Xue, C. Cui, X. Chen, P. Yao, H. Li, *J. Alloy Compd.* **589**, 346 (2014).
- [20] H. Huang, X. Tang, I. Felner, Y. Koltypin, A. Gedanken, *Mater. Res. Bull.* **37**, 1721 (2002).
- [21] L. L. Hench, J. K. West, *Chem. Rev.* **90**, 33 (1990).
- [22] S. M. Ramay, A. Mahmood, S. Atiq, S. A. Siddiqi, S. Naseem, *Materials Today: Proceedings*, **2**, 5485 (2015).
- [23] J. G. Yu, J. C. Yu, W. K. Ho, M. K. P. Leung, B. Cheng, G. K. Zhang, X. J. Zhao, *Appl. Catal. A* **255**, 309 (2003).
- [24] S. Kumar, Y. J. Kim, B. H. Koo, S. K. Sharma, M. Knobel, S. Gautam, K. H. Chae, H. K. Choi, C. G. Lee, *J. Korean Phys. Soc.* **55**, 1060 (2009).
- [25] S. C. Pillai, P. Periyat, R. George, D. E. McCormack, M. K. Seery, H. Hayden, J. Colreavy, *D. Corr, S. J. Hinder, J. Phys. Chem. C* **111**, 1605 (2007).
- [26] D. Jaykrushna, K. Deepa, C. Nonhydrolyti, *J. Phys. Chem. C* **114**, 2544 (2010).
- [27] V. K. Sharma, R. Xalxo, G. D. Varma, *Cryst. Res. Technol.* **42**, 34 (2007).
- [28] D. Wang, S. J. Xiong, *Chin. Phys. Lett.* **25**, 1102 (2008).
- [29] D. J. Priour, E. H. Hwang, S. D. Sarma, *Phys. Rev. Lett.* **92**, 117201 (2004).
- [30] M. Saleem, S. A. Siddiqi, S. M. Ramay, S. Atiq, S. Naseem, *Chin. Phys. Lett.* **29**, 106103 (2012).
- [31] S. V. Bhat, F. L. Deepat, *Solid State Commun.* **135**, 345 (2005).
- [32] Y. Zhang, L. Wu, H. Li, J. Xu, L. Han, B. Wang, Z. Tuo, E. Xie, *J. Alloy Compd.* **473**, 319 (2009).
- [33] M. G. Nair, M. Nirmala, K. Rekha, A. Anukaliani, *Mater. Lett.* **65**, 1797 (2011).
- [34] C. Ruby, K. Ashavani, P. C. Ram, *J. Sol-Gel Sci. Techn.* **63**, 546 (2012).